Journal of Organometallic Chemistry 923 (2020) 121387

Contents lists available at ScienceDirect

Journal of Organometallic Chemistry

journal homepage: www.elsevier.com/locate/jorganchem

Palladium-catalyzed carbonylative synthesis and theoretical study of elongated tubular cavitands

Tímea R. Kégl [a, b, c, *], Tamás Kégl [a, b, c]

[a] Department of Inorganic Chemistry, University of Pécs, Ifjúság útja 6., H-7624, Hungary
[b] János Szentágothai Research Center, Pécs, Ifjúság útja 34., H-7624, Hungary
[c] MTA-PTE Research Group for Selective Chemical Syntheses, Hungary

ARTICLE INFO

Article history:
Received 30 May 2020
Accepted 8 June 2020
Available online 14 July 2020

This paper is dedicated to the 65th birthday of Professor László Kollár, in recognition of his contribution to coordination chemistry, homogeneous catalysis, and carbonylation reactions.

Keywords:
Aminocarbonylation
Homogeneous catalysis
Cavitand
DFT calculations
QTAIM analysis

ABSTRACT

Novel elongated resorcine[4]arene-based tubular cavitands were synthesized via various consecutive reaction steps including homogeneous catalytic carbonylation and cross-coupling processes. The effect of carbon monoxide pressure and different nucleophiles on the selectivity was examined and described. Molecular dynamics and DFT PBEPBE/6-31G(d,p) studies have been carried out for these new deepened cavitand structures to reveal the exact geometry, then QTAIM analysis at B3LYP-D3/def2-TZVP level was performed to shed light on the potential intramolecular weak interactions which have stabilizing effect on the cavitand structures.

1. Introduction

Over the last three decades, supramolecular chemistry has become an intensely developing field. Macromolecules like cavitands possess well-formed large hydrophobic cavity, hence possible applications such as gas sensors, nanoreactors, or drug delivery systems may be considered [1]. The synthesis of macromolecules based on the molecular self-assembly is well-known from biology, in this way numerous novel materials can be prepared. Generally, host molecules are prepared by organic chemical synthetic methods and very few publications can be found in the literature describing homogeneous catalytic syntheses. In recent years, our research group had described several palladium- and copper-catalyzed reactions on a cavitand scaffold [2–5], including the palladium-catalyzed aminocarbonylation [6]. It had been proved that homogeneous catalytic reactions were well adaptable to macromolecules. Comparing to the results of homogeneous catalytic processes carried out on small organic molecules, similar results could have been achieved in terms of both selectivity and reactivity on cavitand scaffolds. In this paper, we perform a palladium-catalyzed aminocarbonylation reaction applied on an elongated cavitand substrate. In this way, carboxamide and ketocarboxamide compounds were synthesized depending on the single or double CO insertion. Carboxamide and ketocarboxamide cavitand derivatives, carrying RC(=O)NHR or RC(=O)NR'R″ groups and large electron-rich inner cavity can act as good molecular selectors for molecules of various biological importance. The larger the size of the internal cavity and the more H-bonding groups the molecule contains, the more likely it will be able to form host-guest complexes. This consideration inspired our research team to synthesize and study particularly large well-functionalized host molecules. To the best of our knowledge, both the substrate and the products are already among the largest synthetic macromolecules.

Altough, theoretical study of these rather large molecules is a considerably complicated and computationally demanding procedure, nowadays the different computational techniques offer excellent additional investigation procedures beside the spectroscopic methods. Molecular dynamics is a very fast tool to find the

* Corresponding author. Department of Inorganic Chemistry, University of Pécs, Ifjúság útja 6., H-7624, Hungary.
E-mail address: trkegl@gamma.ttk.pte.hu (T.R. Kégl).

https://doi.org/10.1016/j.jorganchem.2020.121387

global minimum, furthermore, quantum chemical methods can shed light on the exact geometry and the intra- or even the intermolecular forces as well. The 3D structure and intramolecular weak interactions have also strong influence on the applicability of the host molecule, so the detailed theoretical studies are not avoidable.

2. Results and discussion

2.1. Synthetic studies

Pd-catalyzed aminocarbonylation reaction has previously been accomplished successfully on cavitand scaffolds [6]. Cavitand **1** [2] bearing four iodoaryl groups on the upper rim can be a suitable substrate for various homogeneous catalytic processes as well as aminocarbonylation reaction. Cavitand **1** was synthesized in a seven steps consecutive reaction sequence started with the condensation reaction of 2-methylresorcinol and acetaldehyde [7]. Following steps are the closure of the upper rim via alkylation of the hydroxyl groups [8], radical bromination [9] of the methyl groups on the upper rim, Williamson ether synthesis [10], Sonogashira coupling and copper(I)-catalyzed azide-alkyne cycloaddition (CuAAC) [2]. Although the molar mass of cavitand **1** is above 2000 g/mol (2093.3 g/mol), hence both solubility and steric problems could have been expected during the reaction, successful aminocarbonylation reactions were performed with five different amines (two primary and three secondary amines), at atmospheric and high pressure also. During the reactions *in situ* prepared Pd(0) complex was used as catalyst, triethylamine as base and DMF as solvent. All the high pressure and atmospheric experiments were performed at 60 °C with 48 h reaction time to achieve 100% conversion in each case. The conversion was checked by sampling in the case of atmospheric reactions, but the high pressure experiments also showed complete conversion after 48 h. The reaction scheme is shown in Fig. 1.

Our previous experiences had shown that the selective preparation of the monocarbonylated (carboxamide) product is quite difficult, but the selective preparation of the double carbonylated ketocarboxamide can be carried out at high CO pressure in the presence of high amine excess. Therefore, to promote selectivity, an 18-fold excess of amine (4.5-fold per functional group) was used in the aminocarbonylation process, and the reactions were carried out at 1 and 90 bar CO pressure, respectively. In agreement with our previous results, the high carbon monoxide pressure was favorable for the formation of the ketocarboxamide products, while at atmospheric pressure the carboxyamide products were formed in larger amounts. The best chemoselectivity was observed in the high-pressure experiment with *tert*-butylamine, where 90% of the double carbonylated ketocarboxamide product was obtained (Table 1). Good chemoselectivity was achieved also with *tert*-butylamine, L-alanine methyl ester and pyrrolidine at atmospheric pressure, moreover, with piperidine at high pressure.

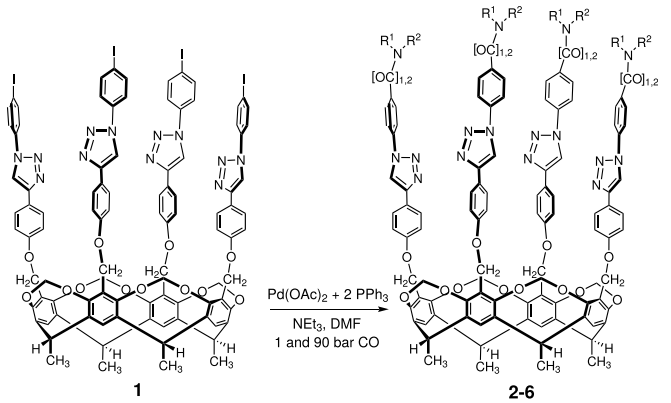

	R^1	R^2		CO 1	CO 2
2	H	*t*-Bu		**a**	**b**
3	$(CH_2)_5$		(Piperidine)	**a**	**b**
4	H	$CH(CH_3)COOCH_3$	(L-Ala-Me-ester)	**a**	**b**
5	$(CH_2)_4O$		(Morpholine)	**a**	**b**
6	$(CH_2)_4$		(Pyrrolidine)	**a**	**b**

Fig. 1. Scheme of the aminocarbonylation reaction accomplished on deepend cavitand scaffold.

The isolation and characterization was performed from product mixture (with the exception of compound **2b**), since the purification of the cavitands by column chromatography and especially the separation of carboxamide and ketocarboxamide products is extremely difficult.

2.2. Theoretical studies

2.2.1. Geometry optimization

Since all our efforts to obtain crystals suitable for X-ray analysis were unsuccessful, theoretical calculations were carried out on **2(a,b)-6(a,b)** to get a deeper insight into the three dimensional structure of these macromolecules. Formerly, a multistep process had been developed [5] by our research team to handle properly these large molecular structures and the cumulating weak interactions. As it had already been mentioned in the Introduction, finding the global minimum for large molecules containing lots of rotable bonds is a considerably complicated and computationally demanding procedure because of the exponentially increasing number of conformers, some of them lying energetically close to each other. Therefore, as first step of our theoretical workflow, molecular dynamics simulations were carried out on cavitand **2(a,b)-6(a,b)** invoking the Schrödinger Suite 2015 MacroModel application. The temperature was chosen 500 K, the equilibration time was 1 ps, the time step was 1.5 fs and the simulation time was 1 ns. OPLS_2005 force field [11], PRCG (Polak-Ribiere Conjugate Gradient) method [12] and chloroform solvent was chosen during the simulations. One thousand conformers were generated for all the structures and the ten lowest energy conformers were sampled to energy minimization in each case.

The results of the molecular dynamics simulations were fully consistent with the NMR spectroscopy data and the lowest energy conformers were highly symmetrical tubular structures close to C_4 symmetry. The higher energy conformers were structurally quite diverse, some of them showed closed but asymmetrical structures, while others exhibited totally opened geometry, where the

Table 1
Products and selectivity values of the aminocarbonylation reactions on cavitand **1**. ('**a**': carboxamide, '**b**': ketocarboxamide compounds.) p[CO] values are in bar, chemoselectivity values in %.

N-nucleophile	p[CO]	Chemoselectivity
tert-Butylamine	1	77 (**2a**) 23 (**2b**)
tert-Butylamine	90	10 (**2a**) 90 (**2b**)
Piperidine	1	53 (**3a**) 47 (**3b**)
Piperidine	90	27 (**3a**) 73 (**3b**)
L-Alanine methyl ester	1	75 (**4a**) 25 (**4b**)
L-Alanine methyl ester	90	35 (**4a**) 65 (**4b**)
Morpholine	1	53 (**5a**) 47 (**5b**)
Morpholine	90	35 (**5a**) 65 (**5b**)
Pyrrolidine	1	70 (**6a**) 30 (**6b**)
Pyrrolidine	90	55 (**6a**) 45 (**6b**)

cavitand branches were drifted away.

Following the molecular dynamics study, further geometry optimization is necessary to assure higher accuracy on geometry. Choosing the most appropriate DFT method is never easy, especially for large macromolecules containing numerous possible weak interactions. Hence, in our previous work [5], a number of methods had been tested to determine which method could present the geometry most consistent with the NMR spectroscopy data. The tested methods were the following: the M06-2X 13, M06-L [13], B97-D3 [14], B3LYP-D3 [15], PBE-D3 and PBEPBE [16] functionals combined with the 6-31G(d,p) [17] basis set. Our experiences had shown that while the structures optimized with PBEPBE function showed near C_4 symmetry, the dispersion corrected methods resulted in distorted geometries. This bad performance of the dispersion corrected functionals for some systems containing cumulating weak interactions is due to that the dispersion correction methods are inclined to overestimate the intramolecular interactions [18].

According to the considerations above the lowest energy conformers obtained by the molecular dynamics simulations were re-optimized at the PBEPBE/6-31G(d,p) [17] level and the wave-function calculations were carried out at the B3LYP-D3 level. Not surprisingly, similarly to the results of molecular dynamics, the geometry re-optimization of all the cavitand structures revealed completely symmetrical (C_4) tubular and slightly helical structures at the PBEPBE/6-31G(d,p) level also.

2.2.2. QTAIM analysis

QTAIM analysis [19] is an excellent and powerful method for investigation not only covalent bonds and charge distribution within a molecule but the different intra- or intermolecular weak interactions also [20–25]. Similarly to chemical bonds, secondary interactions can be well defined with certain QTAIM parameters such as electron density (ρ_{BCP}) at the bond critical point (BCP), its Laplacian ($\nabla^2\rho_{BCP}$) and the total electronic energy density (H_{BCP}).

With these parameters both the strength and the nature of the interactions can be described also. ρ_{BCP} can be correlated with the bond strength, the Laplacian ($\nabla^2\rho_{BCP}$) and the total energy density (H_{BCP}) describe the nature of the bond or interaction. For 'shared-shell' interactions (such as covalent bond) the value of ρ_{BCP} is high and $\nabla^2\rho_{BCP}$ is always negative, while for 'closed-shell' interactions (hydrogen bonds, ionic, donor-acceptor or van der Waals interaction) ρ_{BCP} is much smaller and $\nabla^2\rho_{BCP}$ is positive [26].

The hydrogen bonds can be classified into three distinct groups [22]: 1) strong H-bonds show negative $\nabla^2\rho_{BCP}$, negative H_{BCP} values and covalent character is established, 2) medium H-bonds show positive $\nabla^2\rho_{BCP}$, negative H_{BCP} values and partially covalent character is established, 3) weak H-bonds show positive $\nabla^2\rho_{BCP}$, positive H_{BCP} values and they are mainly electrostatic in nature.

Another approach to describe the strength of an interaction is associated with an other parameter, the interaction energy (E). Espinosa et al. [27] proposed a simple formula to estimate the H-bond energy based on the proportionality between the H-bond energy (E) and the potential electron energy density ($V(\mathbf{r}_{BCP})$) expressed by the following equation where $V(\mathbf{r}_{BCP})$ can be obtained from the topological parameters using the local form of the virial equation:

$$E_{HB} = \frac{1}{2}V(\mathbf{r}_{BCP}) \quad (1)$$

The QTAIM analysis was performed at the B3LYP-D3/def2-TZVP [28] level and the topological parameters are shown in Tables 2–4. The Bader analysis revealed numerous secondary interactions with varying strength (indicated by green dashed line in Figs. 2–11).

Table 2
QTAIM parameters of cavitand **2(a,b)**–**3(a,b)**. ρ_{BCP}, $\nabla^2\rho_{BCP}$ and H_{BCP} values are in atomic unit (au), -E values are in kcal/mol.

Interaction	Cavitand	ρ_{BCP}	$\nabla^2\rho_{BCP}$	H_{BCP}	-E	Distance (Å)
O1···H1	**2a**	0.0114	0.044	0.0020	2.23	2.457
O1···H2	**2a**	0.0046	0.016	0.0008	0.75	2.784
O1···H3	**2a**	0.0083	0.031	0.0017	1.41	2.463
C1···H4	**2a**	0.0047	0.013	0.0006	0.66	2.969
N1···H5	**2a**	0.0104	0.032	0.0014	1.60	2.457
N2···H6	**2a**	0.0038	0.014	0.0008	0.56	2.969
C2···H7	**2a**	0.0043	0.014	0.0007	0.63	2.989
C3···H8	**2a**	0.0052	0.017	0.0008	1.47	2.840
O2···H9	**2a**	0.0099	0.038	0.0017	1.88	2.494
O1···H1	**2b**	0.0260	0.114	0.0024	7.40	2.043
O1···H2	**2b**	0.0065	0.025	0.0014	1.13	2.579
O2···H3	**2b**	0.0070	0.028	0.0015	1.26	2.542
H4···H5	**2b**	0.0037	0.013	0.0008	0.56	2.605
N1···H6	**2b**	0.0114	0.036	0.0016	1.82	2.416
N2···H7	**2b**	0.0036	0.013	0.0008	0.50	3.028
C1···H8	**2b**	0.0039	0.012	0.0006	0.56	3.040
C2···H9	**2b**	0.0049	0.016	0.0008	0.75	2.877
O3···H10	**2b**	0.0104	0.040	0.0018	1.98	2.472
O1···H1	**3a**	0.0075	0.029	0.0015	1.35	2.518
O1···H2	**3a**	0.0088	0.031	0.0014	1.54	2.487
H2···H3	**3a**	0.0042	0.013	0.0008	0.66	2.479
C1···H4	**3a**	0.0027	0.008	0.0005	0.35	3.210
N1···H5	**3a**	0.0066	0.020	0.0009	0.97	2.686
N1···H6	**3a**	0.0037	0.015	0.0009	0.60	2.970
C2···H7	**3a**	0.0048	0.015	0.0007	0.72	2.939
C3···H8	**3a**	0.0055	0.018	0.0008	0.91	2.822
O2···H9	**3a**	0.0095	0.036	0.0016	1.79	2.517
O1···H1	**3b**	0.0150	0.060	0.0023	3.23	2.332
O2···H2	**3b**	0.0135	0.055	0.0023	2.86	2.378
O2···H3	**3b**	0.0087	0.035	0.0018	1.57	2.439
C1···H4	**3b**	0.0044	0.015	0.0008	0.66	2.920
N1···H5	**3b**	0.0072	0.025	0.0011	1.19	2.691
N2···H6	**3b**	0.0037	0.013	0.0008	0.50	3.049
C2···H7	**3b**	0.0034	0.011	0.0006	0.47	3.111
C3···H8	**3b**	0.0043	0.013	0.0007	0.63	2.971
O3···H9	**3b**	0.0100	0.038	0.0017	1.91	2.493

These interactions play a pivotal role in stabilizing the structure and in the formation of the compact tubular geometry. In general, compared to the smaller goblet-shaped derivatives studied earlier [5], these compounds showed a greater number and much stronger interactions according to the ρ_{BCP} and E values.

One of the most significant stabilizing interactions is established between the methylene groups of the lower rigid bowl and the oxygen atoms of the phenoxy groups of the arms. These interactions are the following: O2 – H8 (**6a**), O2 – H9 (**2a, 3a, 5a**), O3 – H9 (**3b, 4a, 5b, 6b**) and O3 – H10 (**2b, 4b**).

Similar stabilizing effect can be attributed to the N – H interactions of the triazole rings (**2a, 3b, 4a, 5b, 6b**: N1 – H5 and N2 – H6, **2b, 4b**: N1 – H6 and N2 – H7, **3a**: N1 – H5 and N1 – H6, **5a, 6a**: N1 – H4 and N1 – H5) and to the O – H interactions associated with the oxygen atoms of the carbonyl groups (**3a, 5a, 6a**: O1 – H1 and O1 – H2, **3b, 5b, 6b**: O2 – H3, **2a**: O1 – H2 and O1 – H3, **2b**: O1 – H2 and O2 – H3, **4a**: O1 – H1 and O2 – H2, **4b**: O1 – H2). These interactions establish electrostatic character in nature because both $\nabla^2\rho_{BCP}$ and $H_{BCP} > 0$. Altough the T-shaped π-stacking interactions, establishing between the phenyl groups of the lower aromatic wall (**2a, 3a, 3b, 4a, 5b, 6b**: C2 – H7 and C3 – H8, **2b, 4b**: C1 – H8 and C2 – H9, **5a**: C3 – H7 and C4 – H8, **6a**: C2 – H6 and C3 – H7), are weaker than the O – H and N – H interactions mentioned above, they still have a considerably contribution to the stabilization of the geometry.

Due to these interactions, the energy of closed (tubular) structures, where the cavitand branches were held together, was always significantly lower than that of open structures.

Table 3
QTAIM parameters of cavitand **4(a,b)**–**5(a,b)**. ρ_{BCP}, $\nabla^2\rho_{BCP}$ and H_{BCP} values are in atomic unit (au), -E values are in kcal/mol.

Interaction	Cavitand	ρ_{BCP}	$\nabla^2\rho_{BCP}$	H_{BCP}	-E	Distance (Å)
O1···H1	**4a**	0.0135	0.051	0.0025	2.45	2.249
O2···H2	**4a**	0.0042	0.015	0.0008	0.69	2.815
O2···H3	**4a**	0.0202	0.101	0.0035	5.74	2.132
C1···H4	**4a**	0.0039	0.011	0.0005	0.53	3.016
N1···H5	**4a**	0.0058	0.020	0.0011	0.91	2.842
N2···H6	**4a**	0.0054	0.018	0.0009	0.82	2.859
C2···H7	**4a**	0.0043	0.013	0.0006	0.63	2.988
C3···H8	**4a**	0.0047	0.015	0.0007	0.69	2.926
O3···H9	**4a**	0.0101	0.038	0.0017	1.91	2.486
O1···H1	**4b**	0.0225	0.110	0.0034	6.65	2.139
O1···H2	**4b**	0.0081	0.032	0.0019	1.44	2.448
O2···H3	**4b**	0.0072	0.028	0.0015	1.26	2.533
H4···H5	**4b**	0.0041	0.015	0.0008	0.63	2.537
N1···H6	**4b**	0.0114	0.036	0.0017	1.82	2.415
N2···H7	**4b**	0.0033	0.012	0.0007	0.47	3.068
C1···H8	**4b**	0.0036	0.011	0.0006	0.50	3.086
C2···H9	**4b**	0.0046	0.015	0.0013	0.72	2.903
O3···H10	**4b**	0.0100	0.038	0.0018	1.88	2.493
O1···H1	**5a**	0.0093	0.036	0.0018	1.69	2.412
O1···H2	**5a**	0.0082	0.029	0.0014	1.41	2.506
C1···H3	**5a**	0.0039	0.012	0.0006	0.53	2.999
C2···H4	**5a**	0.0033	0.011	0.0006	0.47	3.147
N1···H4	**5a**	0.0061	0.018	0.0009	0.88	2.724
N1···H5	**5a**	0.0042	0.016	0.0009	0.66	2.903
C3···H6	**5a**	0.0048	0.015	0.0008	0.72	2.939
C4···H7	**5a**	0.0056	0.019	0.0009	0.91	2.823
O2···H8	**5a**	0.0034	0.014	0.0008	0.56	2.530
O1···H1	**5b**	0.0162	0.065	0.0026	3.54	2.269
O2···H2	**5b**	0.0135	0.055	0.0027	2.86	2.380
O2···H3	**5b**	0.0089	0.035	0.0018	1.60	2.429
C1···H4	**5b**	0.0043	0.014	0.0010	0.63	2.939
N1···H5	**5b**	0.0068	0.023	0.0015	1.10	2.738
N2···H6	**5b**	0.0044	0.015	0.0000	0.66	2.945
C2···H7	**5b**	0.0038	0.011	0.0004	0.50	3.072
C3···H8	**5b**	0.0042	0.013	0.0007	0.63	2.963
O3···H9	**5b**	0.0100	0.038	0.0017	1.88	2.494

Table 4
QTAIM parameters of cavitand **6(a,b)**. ρ_{BCP}, $\nabla^2\rho_{BCP}$ and H_{BCP} values are in atomic unit (au), -E values are in kcal/mol.

Interaction	Cavitand	ρ_{BCP}	$\nabla^2\rho_{BCP}$	H_{BCP}	-E	Distance (Å)
O1···H1	**6a**	0.0068	0.026	0.0013	1.19	2.586
O1···H2	**6a**	0.0124	0.045	0.0020	2.26	2.335
C1···H3	**6a**	0.0037	0.011	0.0005	0.50	3.042
N1···H4	**6a**	0.0065	0.019	0.0009	0.94	2.691
N1···H5	**6a**	0.0035	0.014	0.0009	0.53	2.996
C2···H6	**6a**	0.0044	0.014	0.0007	0.66	2.979
C3···H7	**6a**	0.0054	0.018	0.0008	0.72	2.828
O2···H8	**6a**	0.0099	0.038	0.0017	1.88	2.495
O1···H1	**6b**	0.0155	0.061	0.0023	3.36	2.298
O2···H2	**6b**	0.0155	0.062	0.0024	3.36	2.299
O2···H3	**6b**	0.0090	0.036	0.0019	1.63	2.418
C1···H4	**6b**	0.0043	0.014	0.0007	0.66	2.956
N1···H5	**6b**	0.0074	0.025	0.0012	1.19	2.669
N2···H6	**6b**	0.0036	0.012	0.0008	0.50	3.056
C2···H7	**6b**	0.0035	0.011	0.0006	0.47	3.101
C3···H8	**6b**	0.0043	0.014	0.0007	0.66	2.946
O3···H9	**6b**	0.0102	0.039	0.0018	1.94	2.481

The strongest intramolecular interactions were developed within the cavitand branches (indicated by a pink dashed line in Figs. 2 and 3 and 5–7 and 9 and 11) between the oxygen atoms of the carbonyl groups and the hydrogen atoms of the amine moieties. These 'intra-arm' interactions can play a major role in the funnel-like rigidifying of the upper rim. In the case of derivatives formed with primary amines (**2a, 2b, 4a, 4b**), 1-1 'intra-arm' interaction was found for both the carboxamide and the ketocarboxamide molecule (**2a, 2b, 4b**: O1 – H1 interactions, **4a**: O2 – H3 interaction). On the other hand, for the derivatives formed with secondary amines (**3a, 3b, 5a, 5b, 6a, 6b**) the QTAIM analysis revealed differences between the single and double carbonylated compounds. While no 'intra-arm' interaction was found for the carboxamide compounds (**3a, 5a, 6a**), in the case of ketocarboxamide molecules 2-2 'intra-arm' interactions were identified (**3b, 5b, 6b**: O1 – H1 and O2 – H2 interactions).

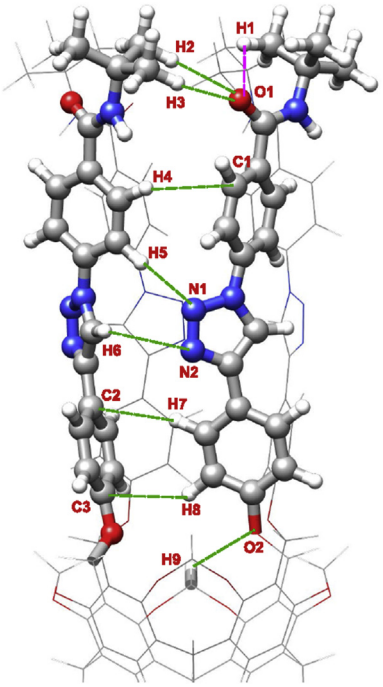

Fig. 2. Structure and weak interactions of cavitand **2a**. Green dashed lines: secondary interactions between the cavitand branches; pink dashed line: 'intra-arm' hydrogen bond. (For interpretation of the references to colour in this figure legend, the reader is referred to the Web version of this article.)

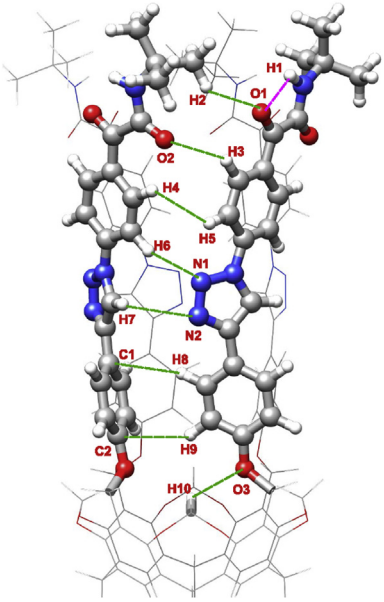

Fig. 3. Structure and weak interactions of cavitand **2b**. Green dashed lines: secondary interactions between the cavitand branches; pink dashed line: 'intra-arm' hydrogen bond. (For interpretation of the references to colour in this figure legend, the reader is referred to the Web version of this article.)

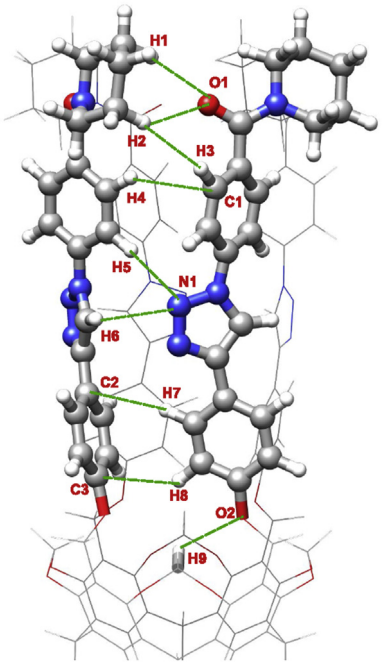

Fig. 4. Structure and weak interactions of cavitand **3a**. Green dashed lines: secondary interactions between the cavitand branches. (For interpretation of the references to colour in this figure legend, the reader is referred to the Web version of this article.)

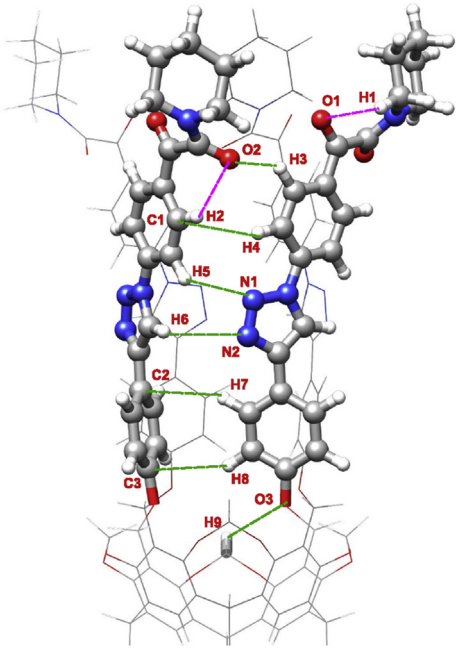

Fig. 5. Structure and weak interactions of cavitand **3b**. Green dashed lines: secondary interactions between the cavitand branches; pink dashed lines: 'intra-arm' hydrogen bonds. (For interpretation of the references to colour in this figure legend, the reader is referred to the Web version of this article.)

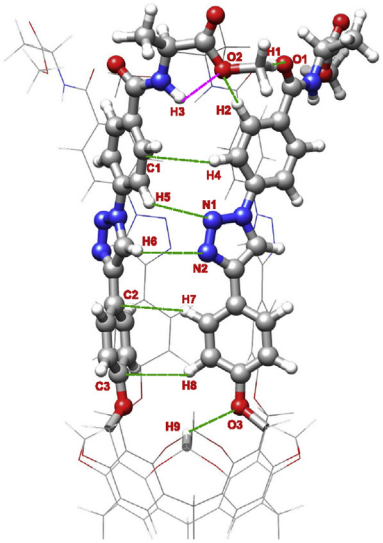

Fig. 6. Structure and weak interactions of cavitand **4a**. Green dashed lines: secondary interactions between the cavitand branches; pink dashed line: 'intra-arm' hydrogen bond. (For interpretation of the references to colour in this figure legend, the reader is referred to the Web version of this article.)

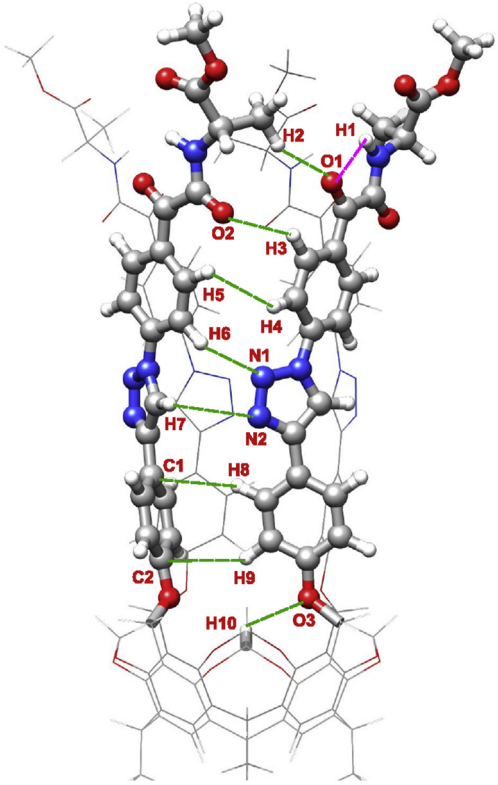

Fig. 7. Structure and weak interactions of cavitand **4b**. Green dashed lines: secondary interactions between the cavitand branches; pink dashed line: 'intra-arm' hydrogen bond. (For interpretation of the references to colour in this figure legend, the reader is referred to the Web version of this article.)

3. Experimental

3.1. General information

Chemicals were either purchased from Sigma-Aldrich. ^{1}H and ^{13}C NMR spectra were recorded at 25 °C in DMSO-d_6 on a 500 MHz Bruker spectrometer. The ^{1}H chemical shifts (δ), reported in parts per million (ppm) downfield to TMS, are referenced to the residual protons (2.50 for DMSO-d_6). The ^{13}C chemical shifts are referenced to the carbon resonance of DMSO-d_6 (39.52 ppm). MALDI-TOF spectra were obtained on an Autoflex II TOF/TOF spectrometer (Bruker Daltonics, Bremen, Germany) in positive ion modes, using a

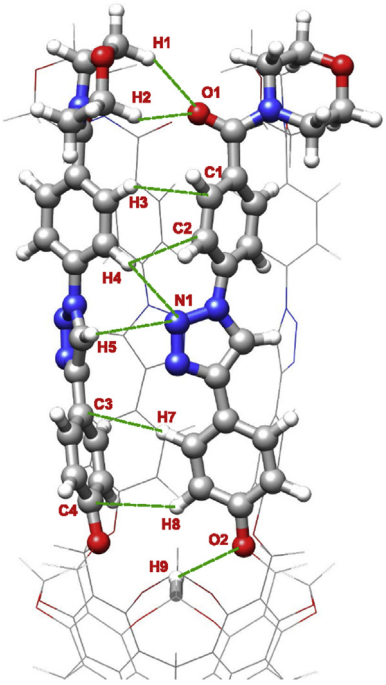

Fig. 8. Structure and weak interactions of cavitand **5a**. Green dashed lines: secondary interactions between the cavitand branches. (For interpretation of the references to colour in this figure legend, the reader is referred to the Web version of this article.)

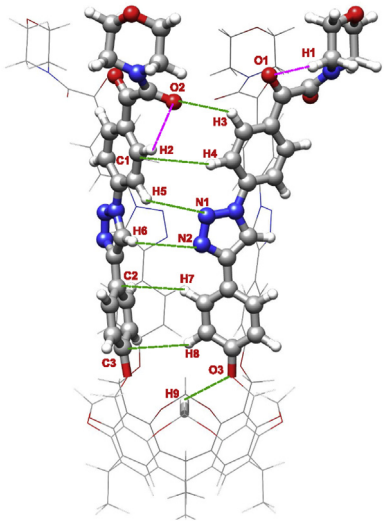

Fig. 9. Structure and weak interactions of cavitand **5b**. Green dashed lines: secondary interactions between the cavitand branches; pink dashed lines: 'intra-arm' hydrogen bonds. (For interpretation of the references to colour in this figure legend, the reader is referred to the Web version of this article.)

337 nm pulsed nitrogen laser (accelerating voltage: 20.0 kV, matrix: DHB). The IR spectra were taken in KBr pellets using an IMPACT 400 spectrometer (Nicolet) applying a DTGS detector in the region of 500–4000 cm^{-1}, the resolution was 4 cm^{-1}. The amount of the samples was ca. 0.5 mg.

3.2. Synthesis and characterization of cavitand ***2(a,b)-6(a,b)***

3.2.1. Atmospheric experiments

Cavitand **1** (100 mg, 0.05 mmol), palladium acetate (2.24 mg,

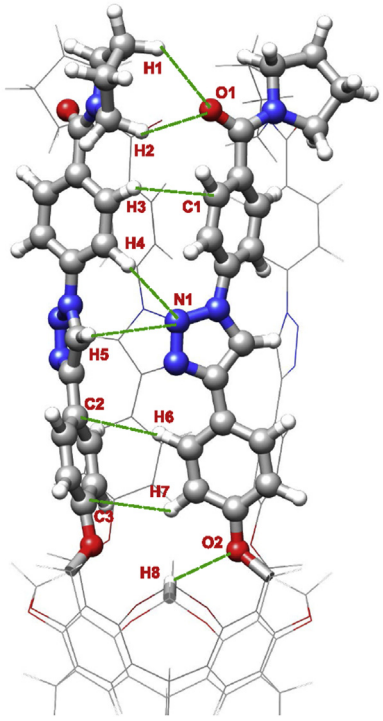

Fig. 10. Structure and weak interactions of cavitand **6a**. Green dashed lines: secondary interactions between the cavitand branches. (For interpretation of the references to colour in this figure legend, the reader is referred to the Web version of this article.)

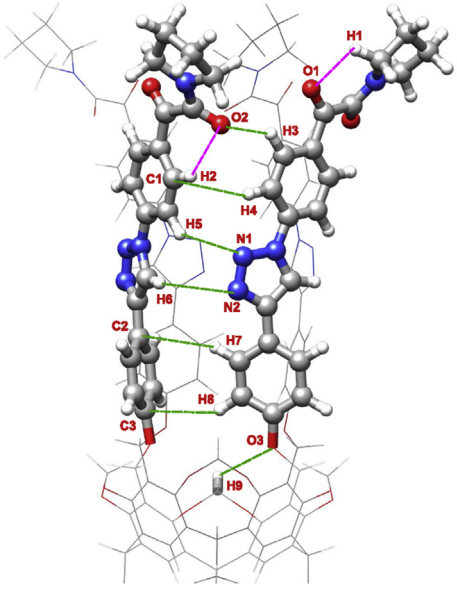

Fig. 11. Structure and weak interactions of cavitand **6b**. Green dashed lines: secondary interactions between the cavitand branches; pink dashed lines: 'intra-arm' hydrogen bonds. (For interpretation of the references to colour in this figure legend, the reader is referred to the Web version of this article.)

0.01 mmol), triphenylphosphine (5.24 mg, 0.02 mmol) and in the case of cavitand **4(a,b)** L-alanine methyl ester (0.9 mmol) were weighed into a three-neck round-bottom flask equiped with a condenser, a magnetic stirrer, a ball filled with argon gas and a vacuum/gas inlet. The solid components were dissolved in dimethylformamide (10 mL) under argon counterflow then the proper liquid amine (0.09 mmol) compounds (*tert*-butylamine for cavitand

2(a,b), piperidine for cavitand **3(a,b)**, morpholine for cavitand **5(a,b)** and pyrrolidine for cavitand **6(a,b)**) and triethylamine base (110 μL, 0.8 mmol) were added to the reaction mixture. Then the argon atmospere was changed to carbon monoxide and the reaction mixture was stirred at 60 °C for 48 h.

The reaction mixture was filtered on filter paper and the solvent was removed with vacuum evaporation. The residue was treated with methanol, the resulting precipitate was collected by filtration and dried in vacuo.

3.2.2. High pressure experiments

Cavitand **1** (100 mg, 0.05 mmol), palladium acetate (2.24 mg, 0.01 mmol), triphenylphosphine (5.24 mg, 0.02 mmol) and in the case of cavitand **4(a,b)** L-alanine methyl ester (0.9 mmol) were weighed into an autoclave. The solid components were dissolved in dimethylformamide (10 mL) under argon counterflow then the proper liquid amine (0.09 mmol) compounds (*tert*-butylamine for cavitand **2(a,b)**, piperidine for cavitand **3(a,b)**, morpholine for cavitand **5(a,b)** and pyrrolidine for cavitand **6(a,b)**) and triethylamine base (110 μL, 0.8 mmol) were added to the reaction mixture. The autoclave was sealed then attached to a carbon monoxide gas cylinder and was placed under 90 bar CO pressure. The reaction mixture was stirred at 60 °C for 48 h.

The reaction mixture was filtered on filter paper and the solvent was removed with vacuum evaporation. The residue was treated with methanol and, the resulting precipitate was collected by filtration and dried in vacuo.

2a: Dark brown powder (45 mg, isolated from product mixture), mp 240–245 °C. IR [cm^{-1}] ν_{max}(KBr): 970.9, 1022, 1090, 1169, 1241, 1296, 1453, 1494, 1620, 2885, 2967 cm^{-1}; ^{1}H NMR (500.15 MHz, DMSO-d_6): 1.41 (36H, s, t-Bu), 1.92 (12H, br s, CH_3CH), 4.57 (4H, br s, inner OCH_2O), 4.93 (8 + 4 H, br s, ArCH_2O + CH_3CH), 5.88 (4H, br s, outer OCH_2O), 7.1 (8H, br s, Ar), 7.62–8.14 (28H, m, Ar), 9.23 (4H, s, C═CH). ^{13}C NMR (125.78 MHz, DMSO-d_6): 16.6 (CH_3CH), 29.04 ((CH_3)$_3$C), 31.8 (CH_3CH), 51.45 ((CH_3)$_3C$), 61.0 (ArCH_2O), 99.95 (OCH_2O), 115.6, 119.3, 119.5, 120, 123.2, 127.3, 129.5, 131.9, 136.04, 138.5, 139.5, 147.8, 153.65, 159.02, 165.6 (N(H)*C*═O).

2b: Light brown powder (17 mg, 32%), mp 245–250 °C. IR [cm^{-1}] ν_{max}(KBr): 975, 1023, 1071, 1094, 1152, 1175, 1245, 1477, 1517, 1603, 1669, 2968, 3396 cm^{-1}; ^{1}H NMR (500.15 MHz, DMSO-d_6): ^{13}C NMR (125.78 MHz, DMSO-d_6): 1.41 (36H, s, t-Bu), 1.94 (12H, d *J* 6.7 Hz, CH_3CH), 4.58 (8H, br s, inner OCH_2O), 4.93 (8 + 4 H, br s, ArCH_2O + CH_3CH), 5.88 (4H, br s, outer OCH_2O), 7.1 (8H, d *J* 7.7 Hz, Ar), 7.47 (8H, br s, Ar), 7.86 (8H, d *J* 7.7 Hz, Ar), 7.95 (4H, s, Ar), 8.14 (8H, br s, Ar), 8.57 (4H, s, NH), 9.3 (4H, s, C = *CH*). ^{13}C NMR (125.78 MHz, DMSO-d_6): 16.04 (CH_3CH), 28.2 ((CH_3)$_3$C), 31.3 (CH_3CH), 51.2 ((CH_3)$_3C$), 60.45 (ArCH_2O), 99.4 (OCH_2O), 115.1, 118.65, 119.8, 122.5, 126.8, 128.6, 128.7, 131.4, 132.0, 139.0, 140.2, 147.5, 153.1, 158.6, 164.9 (N(H)*C*═O), 188.8 (Ar *C*═O). MS: 2098.8 $[M]^+$.

3a: Light brown powder (55 mg, isolated from product mixture), mp 255–260 °C. IR [cm^{-1}] ν_{max}(KBr): 974, 1022, 1241, 1453, 1617, 2851, 2940 cm^{-1}; ^{1}H NMR (500.15 MHz, DMSO-d_6): 1.46 (8 H, br s, (CH_2)-piperidine), 1.63 (16H, br s, (CH_2)$_2$ − piperidine), 1.93 (12H, d *J* 7.0 Hz, CH_3CH), 3.26 (8H, br s, N(CH_2)$_2$), 3.63 (8H, br s, N(CH_2)$_2$), 4.57 (4H, d *J*7.3 Hz, inner OCH_2O), 4.94 (8 + 4 H, br s, ArCH_2O + CH_3CH), 5.88 (4H, d *J* 7.0 Hz, outer OCH_2O), 7.09 (8H, br s, Ar), 7.6 (8H, d *J* 8.5 Hz, Ar), 7.86–8.17 (20H, m, Ar), 9.2 (4H, s, C = *CH*). ^{13}C NMR (125.78 MHz, DMSO-d_6): 16.6 (CH_3CH), 24.5, 25.7, 26.4 (rotamers), 31.1 (CH_3CH), 41.9, 46.8 (rotamers), 61.0 (ArCH_2O), 99.8 (OCH_2O), 115.6, 119.2, 120.2, 123.2, 127.3, 128.8, 131.6, 132.4, 137.4, 139.5, 141.3, 147.7, 153.6, 159.0, 168.3 (N*C*═O–Ar).

3b: Light brown powder (38 mg, isolated from product mixture), mp > 260 °C. IR [cm^{-1}] ν_{max}(KBr): 975, 1010, 1245, 1458, 1636, 2854, 2933 cm^{-1}; ^{1}H NMR (500.15 MHz, DMSO-d_6): 1.47 (8H, br s, (CH_2)-piperidine), 1.64 (16H, br s, (CH_2)$_2$-piperidine), 1.93 (12H, br s, CH_3CH), 3.26 (8H, br s, N(CH_2)$_2$-piperidine), 3.63 (8H, br s, N(CH_2)$_2$-piperidine), 4.58 (4H, br s, inner OCH_2O), 4.93 (8 + 4 H, br s, ArCH_2O + CH_3CH), 5.88 (4H, br s, outer OCH_2O), 7.08 (8H, br s, Ar), 7.47 (8H, m, Ar), 7.86–8.17 (20H, m, Ar), 9.33 (4H, s, C = *CH*). ^{13}C NMR (125.78 MHz, DMSO-d_6): 16.1 (CH_3CH), 23.74, 25.0, 25.8 (rotamers), 31.3 (CH_3CH), 41.4, 46.3 (rotamers), 60.5 (ArCH_2O), 99.4 (OCH_2O), 115.2, 118.7, 120.2, 122.7, 126.9, 128.7, 131.15, 132.1, 133.8, 139.1, 140.8, 147.6, 153.2, 158.6, 164.3 (N*C*═O), 190.8 (Ar*C*═O). MS: 2168.9 $[M+Na]^+$.

4a: Dark brown powder (35 mg, isolated from product mixture), mp > 260 °C. IR [cm^{-1}] ν_{max}(KBr): 967, 1019, 1091, 1244, 1456, 1491, 1620, 1737, 2885, 2947 cm^{-1}; ^{1}H NMR (500.15 MHz, DMSO-d_6): 1.43 (12H, m, CH_3), 1.93 (12H, br s, CH_3CH), 3.6–3.7 (12H, m, CH_3), 4.53 (4 + 4 H, m, inner OCH_2O + alanine *CH* proton), 4.93 (8 + 4 H, br s, ArCH_2O + CH_3CH), 5.89 (4H, br s, outer OCH_2O), 7.09 (8H, br s, Ar), 7.63–8.10 (28H, m, Ar), 9.26 (4H, s, C = *CH*). ^{13}C NMR (125.78 MHz, DMSO-d_6): 16.6 (CH_3CH), 17.2, 31.1 (CH_3CH), 46.3, 48.8, 52.4, 61.0 (ArCH_2O), 99.93 (OCH_2O), 115.6, 119.1, 119.8, 123.2, 127.3, 129.7, 131.9, 133.8, 139.6, 147.9, 153.65, 159.05, 165.63 (N(H)*C*═O), 173.54 (MeO–*C*═O).

4b: Light brown powder (17 mg, isolated from product mixture), mp > 260 °C. IR [cm^{-1}] ν_{max}(KBr): 974, 1444, 1453, 1494, 1596, 1661, 1737, 2947, 2974 cm^{-1}; ^{1}H NMR (500.15 MHz, DMSO-d_6): 1.41 (12H, d *J* 7.2 Hz, CH_3), 1.93 (12H, br s, CH_3CH), 3.62–3.72 (12H, m, CH_3), 4.5 (4 + 4 H, m, inner OCH_2O + alanine *CH* proton), 4.93 (8 + 4 H, br s, ArCH_2O + CH_3CH), 5.88 (4H, br s, outer OCH_2O), 7.08 (8H, br s, Ar), 7.56–8.22 (28H, m, Ar), 9.3 (4H, br s, C = *CH*). ^{13}C NMR (125.78 MHz, DMSO-d_6): 16.6 (CH_3CH), 17.02, 31.8 (CH_3CH), 46.3, 48.1, 52.7, 60.8 (ArCH_2O), 100.1, (OCH_2O), 115.6, 120.2, 123.2, 127.5, 129.3, 132.0, 133.6, 139.6, 140.7, 147.9, 153.6, 159.0, 165.3 (N(H)*C*═O), 172.7(MeO–*C*═O), 189.1 (Ar–*C*═O).

5a: Dark brown powder (58 mg, isolated from product mixture), mp > 260 °C. IR [cm^{-1}] ν_{max}(KBr): 971, 1108, 1244, 1456, 1494, 1597, 1634, 2851, 2967 cm^{-1}; ^{1}H NMR (500.15 MHz, DMSO-d_6): 1.93 (12H, d *J* 6.8 Hz, CH_3CH), 3.56–3.68 (16 + 16 H, m, (CH_2)$_4$-morpholine), 4.58 (4H, br s, inner OCH_2O), 4.93 (8 + 4 H, br s, ArCH_2O + CH_3CH), 5.88 (4H, br s, outer OCH_2O), 7.08 (8H, br s, Ar), 7.48 (8H, br s, Ar), 7.64 (8H, d *J* 8.8 Hz, Ar), 7.86–8.16 (12H, m, Ar), 9.2 (4H, s, C = *CH*). ^{13}C NMR (125.78 MHz, DMSO-d_6): 16.6 (CH_3CH), 32.1 (CH_3CH), 46.4, 61.2 (ArCH_2O), 66.5, 99.9 (OCH_2O), 115.6, 120.2, 120.5, 123.2, 127.3, 127.4, 129.3, 131.9, 132.1, 139.6, 141.3, 148.2, 153.6, 158.9, 168.8 (N*C*═O–Ar).

5b: Brown powder (32 mg, isolated from product mixture), mp > 260 °C. IR [cm^{-1}] ν_{max}(KBr): 971, 1015, 1111, 1210, 1241, 1491, 1596, 1637, 2851, 2964 cm^{-1}; ^{1}H NMR (500.15 MHz, DMSO-d_6): 1.92 (12H, br s, CH_3CH), 3.56–3.68 (16 + 16 H, m, (CH_2)$_4$-morpholine), 4.57 (4H, br s, inner OCH_2O), 4.93 (8 + 4 H, br s, ArCH_2O + CH_3CH), 5.87 (4H, br s, outer OCH_2O), 7.08 (8H, br s, Ar), 7.86–8.15 (28H, m, Ar), 9.32 (4H, s, C = *CH*). ^{13}C NMR (125.78 MHz, DMSO-d_6): 16.6 (CH_3CH), 31.8 (CH_3CH), 46.2, 61.0 (ArCH_2O), 66.6, 99.9 (OCH_2O), 115.6, 119.2, 120.6, 123.2, 127.4, 129.2, 129.7, 131.8, 132.0, 139.6, 141.3, 148.1, 153.6, 159.1, 165.0 (N*C*═O), 190.7 (Ar–*C*═O).

6a: Brown powder (37 mg, isolated from product mixture), mp > 260 °C. IR [cm^{-1}] ν_{max}(KBr): 971, 1090, 1241, 1453, 1494, 1624, 2878, 2967 cm^{-1}; ^{1}H NMR (500.15 MHz, DMSO-d_6): 1.93 (12 + 16 H, m, CH_3CH + pyrrolidine CH_2 proton), 3.43–3.50 (16H, m, (CH_2)$_2$-pyrrolidine), 4.58 (4H, br s, inner OCH_2O), 4.93 (8 + 4 H, br s, ArCH_2O + CH_3CH), 5.88 (4H, br s, outer OCH_2O), 7.07 (8H, br s, Ar), 7.48–8.14 (28H, m, Ar), 9.21 (4H, s, C = *CH*). ^{13}C NMR (125.78 MHz, DMSO-d_6): 16.6 (CH_3CH), 24.4, 26.4 (pyrrolidine rotamers), 31.8 (CH_3CH), 46.5, 49.3 (pyrrolidine rotamers), 61.0 (ArCH_2O), 99.9 (OCH_2O), 115.6, 119.9, 123.2, 127.3, 129.3 (overlapping signals), 132.0, 133.6, 134.9, 137.7, 139.5, 147.8, 153.6, 159.0, 167.5 (N*C*═O–Ar).

6b: Light brown powder (15 mg, isolated from product mixture), mp > 260 °C. IR [cm^{-1}] ν_{max}(KBr): 971, 1022, 1090, 1244, 1456, 1620, 2878, 2964 cm^{-1}; ^{1}H NMR (500.15 MHz, DMSO-d_6): 1.90 (12 + 16 H, m, CH_3CH + pyrrolidine CH_2 proton), 3.43−3.50 (16H, m, $(CH_2)_2$-pyrrolidine), 4.57 (4H, br s, inner OCH_2O), 4.93 (8 + 4 H, br s, ArCH2O + CH_3CH), 5.88 (4H, br s, outer OCH_2O), 7.07 (8H, br s, Ar), 7.47−8.14 (28H, m, Ar), 9.31 (4H, s, C = CH). ^{13}C NMR (125.78 MHz, DMSO-d_6): 16.6 (CH_3CH), 24.2, 26.2 (pyrrolidine rotamers), 31.8 (CH_3CH), 46.7, 49.3 (pyrrolidine rotamers), 61.0 (ArCH_2O), 99.9 (OCH2O), 115.6, 119.9, 123.5, 127.3, 129.3 (overlapping signals), 132.0, 133.6, 134.9, 137.7, 139.5, 148.0, 153.6, 159.2, 164.4 (NC═O), 190.9 (Ar−C═O).

3.3. Computational details

The geometry of **2(a,b)-6(a,b)** were calculated without any symmetry constraints at all levels of theory employed in this study. For the stationary points, the Hessian was evaluated to characterize the genuine minimum (no imaginary frequencies). Molecular dynamics simulations were carried out with the Schrödinger Suite 2015 MacroModel application using the OPLS_2005 force field [11] and the PRCG (Polak-Ribiere Conjugate Gradient) method [12]. For the geometry re-optimization at the PBEPBE/6-31G(d,p) [16,17] level and the electronic structure calculation at the B3LYP-D3/def2-TZVP [15,28] level the Gaussian 09.D01 suite of programs was used [29]. QTAIM analyses were carried out with the AIMAll [30] software to investigate the electron density of the optimized structures.

4. Conclusions

Palladium-catalyzed aminocarbonylation process was implemented on highly extended cavitand scaffold, thereby valuable carboxamide and ketocarboxamide host molecules were successfully synthesized. According to the catalytic studies, high CO pressure was favorable for double carbonylation reaction and forming ketocarboxamide products while atmospheric pressure resulted in rather carboxamide compounds formed by single CO insertion. Theoretical studies revealed a specific tubular and slightly helical 3D structure for all these molecules which are stabilized and rigidified by numerous intramolecular weak interactions. These interactions are mainly electrostatic in nature but some of them show van der Waals character.

Declaration of competing interest

The authors declare that they have no known competing financial interests or personal relationships that could have appeared to influence the work reported in this paper.

Acknowledgments

This work has been supported by the GINOP-2.3.2-15-2016-00049 grant and the European Social Fund Grant no.: EFOP-3.6.1.-16-2016-00004 entitled by Comprehensive Development for Implementing Smart Specialization Strategies at the University of Pécs.

Appendix A. Supplementary data

Supplementary data to this article can be found online at https://doi.org/10.1016/j.jorganchem.2020.121387.

References

[1] D.J. Cram, J.M. Cram, Container Molecules and Their Guests, Royal Society of Chemistry, 1997.
[2] Z. Csók, T. Kégl, Y. Li, R. Skoda-Földes, L. Kiss, S. Kunsági-Máté, M.H. Todd, L. Kollár, Tetrahedron 69 (2013) 8186−8190.
[3] D. Filotás, L. Nagy, T.R. Kégl, Z. Csók, L. Kollár, G. Nagy, Electroanalysis 27 (2015) 799−807.
[4] T.Z. Jánosi, G. Makkai, T. Kégl, P. Mátyus, L. Kollár, J. Erostyák, J. Fluoresc. 26 (2016) 679−688.
[5] T. Kégl, G. Csekő, G. Mikle, A. Takátsy, L. Kollár, T. Kégl, Chemistry 2 (2017) 8337−8345.
[6] Z. Csók, A. Takátsy, L. Kollár, Tetrahedron 68 (2012) 2657−2661.
[7] L.M. Tunstad, J.A. Tucker, E. Dalcanale, J. Weiser, J.A. Bryant, J.C. Sherman, R.C. Helgeson, C.B. Knobler, D.J. Cram, J. Org. Chem. 54 (1989) 1305−1312.
[8] E. Román, C. Peinador, S. Mendoza, A.E. Kaifer, J. Org. Chem. 64 (1999) 2577−2578.
[9] T.N. Sorrell, F.C. Pigge, J. Org. Chem. 58 (1993) 784−785.
[10] Z. Csók, T. Kégl, L. Párkányi, Á. Varga, S. Kunsági-Máté, L. Kollár, Supramol. Chem. 23 (2011) 710−719.
[11] J.L. Banks, H.S. Beard, Y. Cao, A.E. Cho, W. Damm, R. Farid, A.K. Felts, T.A. Halgren, D.T. Mainz, J.R. Maple, et al., J. Comput. Chem. 26 (2005) 1752−1780.
[12] L. Grippo, S. Lucidi, Math. Program. 78 (1997) 375−391.
[13] Y. Zhao, D.G. Truhlar, Theor. Chem. Acc. 120 (2008) 215−241.
[14] S. Grimme, S. Ehrlich, L. Goerigk, J. Comput. Chem. 32 (2011) 1456−1465.
[15] A.D. Becke, J. Chem. Phys. 98 (1993) 5648−5652.
[16] J.P. Perdew, K. Burke, M. Ernzerhof, Phys. Rev. Lett. 77 (1996) 3865.
[17] W.J. Hehre, R. Ditchfield, J.A. Pople, J. Chem. Phys. 56 (1972) 2257−2261.
[18] N. Pálinkás, L. Kollár, T. Kégl, Dalton Trans. 46 (2017) 15789−15802.
[19] R. Bader, T. Nguyen-Dang, Adv. Quantum Chem. 14 (1981) 63−124.
[20] M.D. Esrafili, J. Mol. Model. 18 (2012) 5005−5016.
[21] J. Perlstein, K. Steppe, S. Vaday, E.M.N. Ndip, J. Am. Chem. Soc. 118 (1996) 8433−8443.
[22] I. Rozas, I. Alkorta, J. Elguero, J. Am. Chem. Soc. 122 (2000) 11154−11161.
[23] S.J. Grabowski, Chem. Rev. 111 (2011) 2597−2625.
[24] H. Zhou, W.-P. Lai, Z. Zhang, W.-K. Li, H.-Y. Cheung, J. Comput. Aided Mol. Des. 23 (2009) 153−162.
[25] L. Seridi, A. Boufelfel, S. Soltani, J. Mol. Liq. 221 (2016) 885−895.
[26] R. Bader, Atoms in Molecules: A Quantum Theory, 1990.
[27] E. Espinosa, E. Molins, C. Lecomte, Chem. Phys. Lett. 285 (1998) 170−173.
[28] F. Weigend, R. Ahlrichs, Phys. Chem. Chem. Phys. 7 (2005) 3297−3305.
[29] M.J. Frisch, G.W. Trucks, H.B. Schlegel, G.E. Scuseria, M.A. Robb, J.R. Cheeseman, G. Scalmani, V. Barone, B. Mennucci, G.A. Petersson, H. Nakatsuji, M. Caricato, X. Li, H.P. Hratchian, A.F. Izmaylov, J. Bloino, G. Zheng, J.L. Sonnenberg, M. Hada, M. Ehara, K. Toyota, R. Fukuda, J. Hasegawa, M. Ishida, T. Nakajima, Y. Honda, O. Kitao, H. Nakai, T. Vreven, J.A. Montgomery Jr., J.E. Peralta, F. Ogliaro, M. Bearpark, J.J. Heyd, E. Brothers, K.N. Kudin, V.N. Staroverov, R. Kobayashi, J. Normand, K. Raghavachari, A. Rendell, J.C. Burant, S.S. Iyengar, J. Tomasi, M. Cossi, N. Rega, J.M. Millam, M. Klene, J.E. Knox, J.B. Cross, V. Bakken, C. Adamo, J. Jaramillo, R. Gomperts, R.E. Stratmann, O. Yazyev, A.J. Austin, R. Cammi, C. Pomelli, J.W. Ochterski, R.L. Martin, K. Morokuma, V.G. Zakrzewski, G.A. Voth, P. Salvador, J.J. Dannenberg, S. Dapprich, A.D. Daniels, Ö. Farkas, J.B. Foresman, J.V. Ortiz, J. Cioslowski, D.J. Fox, Gaussian 09 Revision D.01, Gaussian Inc., Wallingford CT, 2009.
[30] T.A. Keith, AIMAll (Version 19.02.13), TK Gristmill Software, Overland Park KS, USA, 2019, 2019 (aim.tkgristmill.com).